Yield stress fluids method to determine the pore size distribution of a porous medium

A. Oukhlef, S. Champmartin, A. Ambari *

Arts et Métiers ParisTech, 2 bd du Ronceray, Angers, France

Keywords:
Pore-size distribution
Non-Newtonian yield stress fluids
Porous media

A B S T R A C T

In this paper a new method is presented in order to determine the pore size distribution in a porous medium. This original technique uses the rheological properties of some non-Newtonian yield stress fluids flowing through the porous sample. This technique is based on the capillary bundle model (like the other classical methods) which, despite its apparent simplicity, is capable of properly characterizing the percolating pore size distribution. Then this distribution can be simply obtained from the measurement of the total flow rate as a function of the imposed pressure gradient. The present technique is successfully tested analytically and numerically for usual pore size distributions such as the Gaussian mono and multimodal distributions, using Bingham and Casson fluids. The technique can also be extended to any yield stress fluid and any kind of distribution.

1. Introduction

Porous media are found literally everywhere around us [1–4], in living matter, in Nature and in various technological applications. The need in porous media will keep on growing in the future because of the increase in the price of energy and because of environmental challenges; let us cite for example the recent application of heat storage in granular porous media for solar collectors [5]; another instance concerns heat storage for human housing using porous phase change materials [6]; the continuous decrease in conventional oil and gas reserves implies a high level of investments for tertiary recovery techniques [7]; the storage and the behavior of pollutants in porous matter (hazardous wastes, CO_2 sequestration...) are today an important challenge; they are also used in some biological processes (dialysis, membrane transport) [8]... These numerous applications make them the object of abundant studies and are topics for which it is essential to have an in-depth knowledge and an accurate characterization.

Since the early work of Darcy [9], the transport phenomena in general and particularly the flow through porous media generated an important research activity which is today still relevant. In fact, all the porous media are made of networks of pores delimited by a solid. Among the pores constituting this network we are particularly interested in the percolating conduits excluding the isolated pores, the dead ends and the finite clusters which do not carry any flow. In these conditions the characterization of the percolating pore size distribution (PSD) of these porous media is a crucial goal [10]. In fact the strong dependence of the transport properties in porous media with the size of their pores and their polydispersity constitute a challenge in many scientific areas. Various techniques have been developed to characterize the network of such porous solids, and particularly their pore size distribution. Among the most popular techniques, we can quote: the mercury intrusion porosimetry (MIP) [1–3,11] consisting into the injection of mercury in the porous medium. This technique is based on the existence of a threshold below which the pores cannot be invaded. Indeed due to its large surface tension mercury does not wet most of the materials. A pressure difference ΔP_{lg} must be imposed so that mercury penetrates the pores whose radii r_p are greater than $r_p^* = 2\sigma_{lg}\cos\theta/\Delta P_{lg}$ where σ_{lg} is the liquid/gas interfacial tension and θ the contact angle. The pore size volume distribution is obtained with the derivative of the curve representing the volume of the invaded pores according to the radius of the pores. Because of the toxicity of mercury, this technique is intended to be phased out. Another method to measure the pore-size distributions is the BJH. method [12]. This classical method uses two mechanisms: the isothermal adsorption (of nitrogen at 77 K) on the pore walls and the capillary condensation, due to the molecular Van der Waals interactions between a condensing vapor and the internal surface of the pores. This BJH technique is based on the relationship between the imposed pressure and the radius of a cylindrical pore where the capillary condensation takes place. This is the Kelvin–Laplace equation: $\ln(P/P_0) = -2\sigma_{lg}\upsilon_l\cos\theta/NkTr_p$, where P and P_0 are respectively the partial vapor pressure, the saturation vapor pressure at the temperature T, r_p the pore radius, N the Avogadro's number, k the Boltzmann's constant and υ_l the liquid phase molar volume. This method consists in measuring the desorption volume

* Corresponding author. Tel./fax: +33 241207362.
E-mail address: ambari@ensam.eu (A. Ambari).

http://dx.doi.org/10.1016/j.jnnfm.2013.12.004

vs. the relative pressure: P/P_0. Then the pore size distribution is obtained from the derivative of this curve.

An alternative technique rests on the liquid–solid phase transition of the fluid in a porous medium [13,14]. This approach for determining the PSD in porous materials has been suggested by Kuhn et al. [15] and derived later by Brun et al. [16]. The principle of the method is based on the lowering of the triple point temperature of a liquid filling a porous material. It uses a thermodynamical relationship between the reduction of the triple point temperature ΔT of the confined liquid in the pores of radius r_p where the phase transition occurs. It is expressed by the Gibbs–Thomson equation: $\Delta T/T_0 = 2\sigma_{ls}v_l/\Delta H_0 r_p$, where σ_{ls} is the liquid/solid interfacial tension, v_l the liquid phase molar volume, ΔH_0 the molar heat of fusion, r_p the pore radius, and T_0 the triple point temperature of the unconfined liquid. Then the phase transitions (solidification or melting) for a liquid confined within a pore occur at lower temperatures when the pore size decreases. This difference in transition temperature ΔT, between confined and bulk liquid can be measured calorimetrically by DSC thermoporometry (differential scanning calorimetry) [17] or cryoporometry using nuclear magnetic resonance (NMR) [18]. Notice that all the techniques mentioned above and developed in order to measure the pore size distribution are based on the existence of a threshold. The first one is due to the capillary pressure; the two others are due to the phase change phenomena. Finally let us quote destructive techniques such as stereology [19] or non-destructive methods such as Small Angle Neutron (SANS) or X-Ray Scattering (SAXS) [20,21]. Unfortunately all these techniques can give quite different results; moreover they are very expensive and require complex equipment. Therefore in this study we propose a new alternative, simpler and cheaper technique, in order to characterize the PSD of a porous medium.

2. Objective of the study

Starting from the same principle utilized in the first three thermodynamical methods described above, we develop an approach based on the threshold introduced by a yield stress fluid (which belongs to the class of non-Newtonian viscoplastic fluids without time dependence). These fluids do not flow, before being subject to a minimum shear stress called the flow yield stress τ_0. Many materials such as polymers (carbopol…), foodstuffs (mayonnaise…), cosmetics (beauty cream, toothpaste…), concentrated slurries, electro-rheological fluids (suspensions of very fine conducting particles in an electrically insulating fluid) and magneto-rheological fluids (suspensions of magnetically polarizable micron-sized particles in oil) [22]… have a rheological behavior which is situated between a purely viscous liquid and a plastic solid. These fluids may have a more or less well defined yield stress. This critical stress that accompanies the transition between the solid and the viscous behaviors is related to the internal structure of the network of the material. The magnitude of the yield stress may depend on the concentration of the dissolved substances inducing the threshold and it may also vary with the pH of the solution (like bentonite [23]). A lot of behavior laws are available to describe such complex fluids. In our study we focus only on the classical Bingham fluids [24,25] (drilling muds, oil painting, Laponite [26]…), and Casson fluids (printing ink [27], sludge suspensions and dispersion paint, blood [28]…).

The basic idea is the following: in order to set such fluids into motion, it is necessary to impose between both ends of a pore a pressure gradient (∇P) greater than a critical value depending on the fluid yield stress (τ_0) and the pore radius (r_p). In other words, for the pressure gradient ∇P, only the pores whose radius is greater than the critical radius $r_0 = 2\tau_0/\nabla P$ are invaded. Then it is possible to scan the PSD by increasing the pressure gradient step by step and measuring the corresponding flow rate Q.

3. Models and procedure

3.1. Porous medium and yield stress fluid models

In order to determine the pore size distribution of the percolating pores, the most popular model in all the thermodynamical techniques described above is the capillary bundle model [29,30]. Although it is quite simple, it can account for most of the geometrical properties of the real porous media such as the tortuosity, the permeability and the variation in the pore cross-section as we shall see later. Nevertheless the interconnectivity cannot be modeled. We will use this model to derive the inversion technique which allows us to obtain the PSD from the characteristic curve $Q = f(\nabla P)$ for a given yield stress fluid in non-inertial regimes. The simplest yield stress fluid is described by the Bingham model. Such a fluid obeys the following rheological behavior law:

$$\begin{cases} \underline{\underline{\tau}} = 2\left(\eta + \dfrac{\tau_0}{\sqrt{2\,\underline{\underline{D}}:\underline{\underline{D}}}}\right)\underline{\underline{D}} & \text{for } \sqrt{\dfrac{\underline{\underline{\tau}}:\underline{\underline{\tau}}}{2}} > \tau_0 \\ \underline{\underline{D}} = 0 & \text{for } \sqrt{\dfrac{\underline{\underline{\tau}}:\underline{\underline{\tau}}}{2}} \leqslant \tau_0 \end{cases} \tag{1}$$

with $\underline{\underline{\tau}}$ the shear stress tensor, $\underline{\underline{D}}$ the rate of deformation tensor and η the plastic viscosity of the fluid. For the flow in a tube with circular cross-section, these equations take the simpler form:

$$\begin{cases} \tau_{r'z} = \tau_0 + \eta\left|\dfrac{\partial u_z}{\partial r'}\right| & \text{for } \tau_{r'z} > \tau_0 \\ \dfrac{\partial u_z}{\partial r'} = 0 & \text{for } \tau_{r'z} \leqslant \tau_0 \end{cases} \tag{2}$$

where $\tau_{r'z}$ is the shear stress, $(\partial u_z/\partial r')$ the rate of deformation and r' is the radial coordinate.

3.2. Procedure and inversion

Our model is composed of parallel capillaries (Fig. 1) whose radii are distributed according to the unknown probability density function $p(r)$. When a pressure gradient ∇P is imposed on this system, the total flux is calculated from the elementary flow rate $q(\nabla P, r)$ in a single capillary of radius r and from $p(r)$ by the integral:

$$Q(\nabla P) = \int_{r_0=\frac{2\tau_0}{\nabla P}}^{\infty} q(\nabla P, r)p(r)\,dr \tag{3}$$

This integral constitutes a Volterra equation of the first kind. As long as the regime is non-inertial, the kernel of Eq. (3) is given by [31]:

$$q(\nabla P, r) = \begin{cases} \dfrac{\pi\tau_0 r^4}{4\eta r_0}\left[1 - \dfrac{4}{3}\left(\dfrac{r_0}{r}\right) + \dfrac{1}{3}\left(\dfrac{r_0}{r}\right)^4\right] & \text{for } r > r_0 \\ 0 \text{ for } r \leqslant r_0 \end{cases} \tag{4}$$

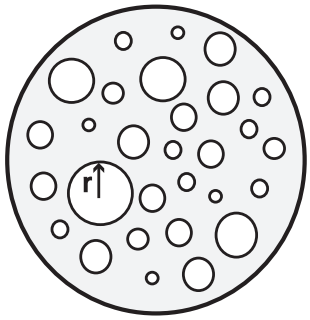

Fig. 1. Capillary bundle model.

For $r \leqslant r_0$ the fluid does not flow. The critical radius $r_0 = 2\tau_0/\nabla P$ is also the radius of the core zone of the Bingham plug flow (Fig. 2).

The pore size distribution $p(r)$ can be obtained through differential operators applied to $Q(\nabla P)$ [32,33]:

$$p(r) = \frac{\eta(\nabla P)^2}{\pi\tau_0 r^4}\left[5\frac{\partial^2.}{\partial(\nabla P)^2} + \nabla P\frac{\partial^3.}{\partial(\nabla P)^3}\right]Q|_{\nabla P=\frac{2\tau_0}{r}} \tag{5}$$

3.3. Validation

As encountered usually in Nature and literature, the pore size distributions may be approximated by Gaussian mono-modal or multimodal (bi or tri-modal) distributions [34] and such PSD will be considered in this article. Note that the log-normal or Maxwellian distributions [12] are sometimes used but they are not considered here. To verify the applicability of formula (5), let us assume that the PSD can be described by a given Gaussian distribution of mean value μ and standard deviation σ. In order to remain as general as possible and exhibit the control parameters of this problem, we will write from now on the equations in non-dimensional form:

$$p^+(r^+) = \frac{1}{\sigma^+\sqrt{2\pi}}\exp\left[-\frac{(r^+-\mu^+)^2}{2\sigma^{+2}}\right] \tag{6}$$

where $r^+ = r/L$, $p^+(r^+) = L\cdot p(r)$, $\sigma^+ = \sigma/L$, $\mu^+ = \mu/L$, and L the thickness of the studied sample. As the other natural scales of the material are a priori unknown, we use this thickness L as the length scale because it is the most accessible dimension of the system. $\dot\gamma_c = \eta/(\rho L^2)$ is the characteristic shear rate scale and ρ the fluid density. The non-dimensional rheological behavior law is then written as:

$$\begin{cases} \tau^+_{r'z} = 1 + \frac{1}{He}\left|\frac{\partial u^+_z}{\partial r'^+}\right| \text{ for } \tau^+_{r'z} > 1 \\ \frac{\partial u^+_z}{\partial r'^+} = 0 \text{ for } \tau^+_{r'z} \leqslant 1 \end{cases} \tag{7}$$

with $\tau^+_{r'z} = \tau_{r'z}/\tau_0$ the adimensional shear stress and the Hedström number He [35] given by:

$$He = \frac{\rho\tau_0 L^2}{\eta^2} \tag{8}$$

This non-dimensional number represents the relative importance of the yield stress to the viscous one. The adimensional rheograms for a Bingham fluid at different He is shown in Fig. 3.

Now, it is possible to normalize the Volterra equation (Eq. (3)) as follows:

$$Q^+(\nabla P^+) = \int_{r_0^+=\frac{2}{\nabla P^+}}^{\infty} q^+(\nabla P^+, r^+)p^+(r^+)\,dr^+ \tag{9}$$

where the flow rate is normalized by $Q_c = \pi\eta L/8\rho$ and the pressure gradient is normalized by $\nabla P_c = \tau_0/L$. The non-dimensional elementary flow rate in a single capillary tube is:

$$q^+(\nabla P^+, r^+) = \begin{cases} He\left[\nabla P^+(r^+)^4 - \frac{8}{3}(r^+)^3 + \frac{16}{3}\frac{1}{(\nabla P^+)^3}\right] & \text{for } r^+ > r_0^+ \\ 0 \quad \text{for } r^+ \leqslant r_0^+ \end{cases} \tag{10}$$

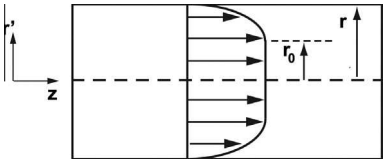

Fig. 2. Bingham flow through a pore of radius r.

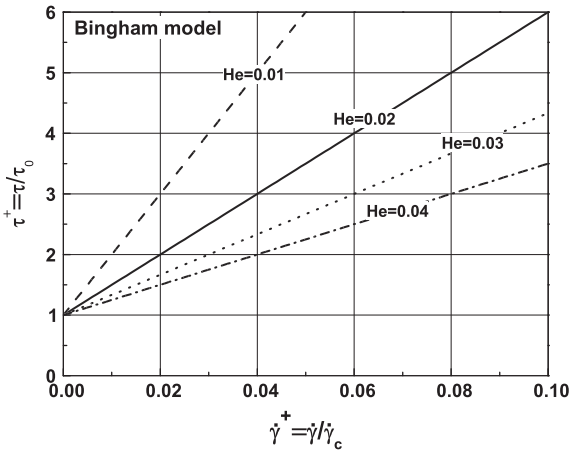

Fig. 3. Bingham fluid rheograms for different He.

The adimensional PSD (5) can now be written as follows:

$$p^+(r^+) = \frac{(\nabla P^+)^6}{128He}\left[5\frac{\partial^2.}{\partial(\nabla P^+)^2} + \nabla P^+\frac{\partial^3.}{\partial(\nabla P^+)^3}\right]Q^+|_{\nabla P^+=\frac{2}{r^+}} \tag{11}$$

Eq. (11) is called the "Pore Size Distribution Equation" or PSDE. In a first step, we use a given Gaussian PSD calculated by Eq. (6) for $\sigma^+ = 2\cdot 10^{-5}$ and $\mu^+ = 10^{-4}$. Fig. 4 below shows the normalized total flow rate vs. the normalized pressure gradient resulting from the flow of the Bingham fluid through such a porous medium. This flow rate is calculated by Eq. (9). This figure is characterized by a first region at low pressure gradients in which the flow rate is zero. This region extends until the largest pore in the material is invaded. It is followed by a second region in which the flow rate increases with the pressure gradient.

In a second step, the given distribution is forgotten and the flow rate vs. pressure gradient (or the characteristic curve) given by the initial calculation (or obtained by an experiment) is used as a starting point. Now, Eq. (11) is applied to the non-dimensional characteristic curve to calculate $p^+(r^+)$ which is plotted in Fig. 5 (obtained from real data corresponding to $He = 0.02$ with $\rho = 10^3$ kg m^{-3}, $\tau_0 = 20$ Pa, $\eta = 10$ Pa s, $L = 10^{-2}$ m). Notice that this non-dimensional characteristic curve depends only on the PSD but not on He. Indeed as the non-dimensional pore size distribution given by Eq. (11) is inversely proportional to He and the non-dimensional elementary flow rate q^+ is proportional to He (see Eq. (10)), He vanishes and does not affect the curve $Q^+ = f(\nabla P^+)$ according to Eq. (9).

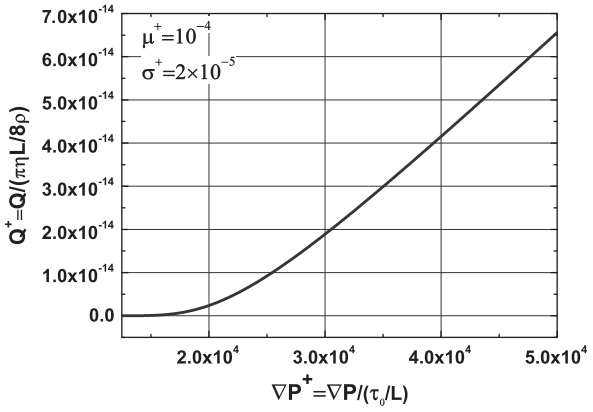

Fig. 4. Total flow rate vs. pressure gradient for a Gaussian distribution and a Bingham fluid.

This figure exhibits a perfect agreement between the original Gaussian distribution and the one calculated with the relationship obtained for $p^+(r^+)$ by the inverse method. To verify the efficiency of this technique with more complex distributions, a bimodal Gaussian distribution is considered, with two peaks at $\mu_1^+ = \mu_1/L$ and $\mu_2^+ = 2\mu_1^+$ and different standard deviations $\sigma_2^+ = 2\sigma_1^+ = \sigma_2/L$ for instance such as:

$$p^+(r^+) = \frac{1}{2}\left[\frac{1}{\sigma_1^+\sqrt{2\pi}}\exp\left(-\frac{(r^+-\mu_1^+)^2}{2(\sigma_1^+)^2}\right) + \frac{1}{\sigma_2^+\sqrt{2\pi}}\exp\left(-\frac{(r^+-\mu_2^+)^2}{2(\sigma_2^+)^2}\right)\right] \tag{12}$$

in which the radius and the PSD are also scaled by L. The total flow rate Q^+ is also obtained and shown in Fig. 6. Now, Eq. (11) is applied again to the non-dimensional characteristic curve (Fig. 6). The result is plotted in Fig. 7. Once again one can see the perfect agreement between the initial PSD and the one calculated by Eq. (11).

Finally, for a more complex tri-modal distribution with for example: $\mu_2^+ = 2\mu_1^+$, $\mu_3^+ = 3\mu_1^+$ and $\sigma_2^+ = 3\sigma_1^+/2$, $\sigma_3^+ = 2\sigma_1^+$ the non-dimensional characteristic curve (Fig. 8), is obtained and once again the application of the PSDE gives with accuracy the initial density probability function as shown in Fig. 9.

3.4. Casson model

As the results obtained with the Bingham model are very encouraging and since it is difficult to find a fluid having the ideal Bingham behavior, we apply in the next section the analysis to another yield stress fluid: the Casson model that is more frequent than the Bingham fluid. For this occasion, we check the independence of the analysis on the chosen rheological law. In this model the general rheological behavior law can be written as:

$$\begin{cases} \underline{\underline{\tau}} = 2\left[\eta^{1/2} + \left(\frac{\tau_0}{\sqrt{2\underline{\underline{D}}:\underline{\underline{D}}}}\right)^{1/2}\right]^2 \underline{\underline{D}} & \text{for } \sqrt{\frac{\underline{\underline{\tau}}:\underline{\underline{\tau}}}{2}} > \tau_0 \\ \underline{\underline{D}} = 0 \quad \text{for} \quad \sqrt{\frac{\underline{\underline{\tau}}:\underline{\underline{\tau}}}{2}} \leqslant \tau_0 \end{cases} \tag{13}$$

As in the previous section, these equations reduce to the following simpler forms in the case of the shear flow in a circular tube:

$$\begin{cases} \tau_{r'z}^{1/2} = \tau_0^{1/2} + \eta^{1/2}\left|\frac{\partial u_z}{\partial r'}\right|^{1/2} \text{ for } \tau_{r'z} > \tau_0 \\ \frac{\partial u_z}{\partial r'} = 0 \quad \text{for } \tau_{r'z} \leqslant \tau_0 \end{cases} \tag{14}$$

The elementary flow rate in a circular capillary tube constituting the kernel of Eq. (3) can be written as in [36]:

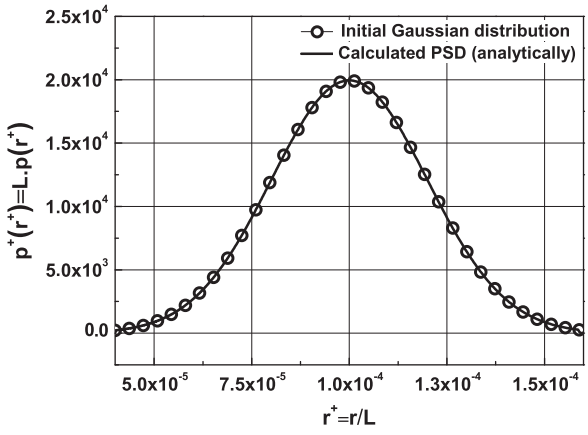

Fig. 5. Comparison between the initial and the calculated PSD.

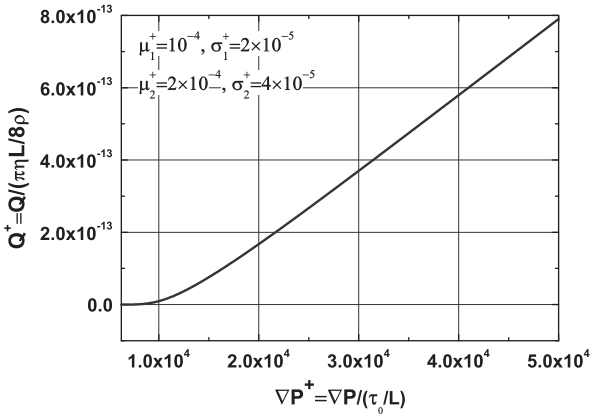

Fig. 6. Total flow rate vs. pressure gradient for a bimodal distribution with $\mu_2^+ = 2\mu_1^+$, $\sigma_2^+ = 2\sigma_1^+$ and a Bingham fluid.

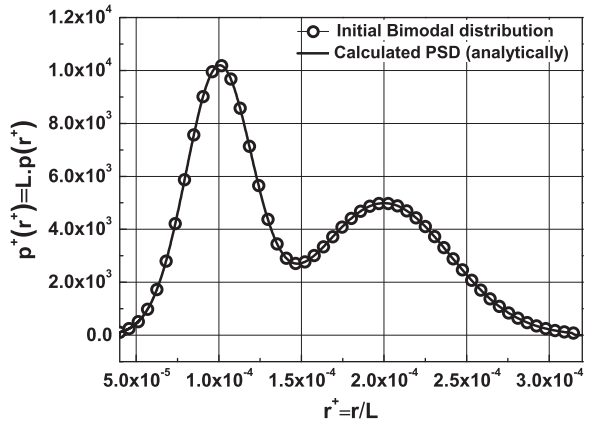

Fig. 7. Comparison between the initial and the calculated PSD for a bimodal distribution with $\mu_2^+ = 2\mu_1^+$, $\sigma_2^+ = 2\sigma_1^+$ and a Bingham fluid.

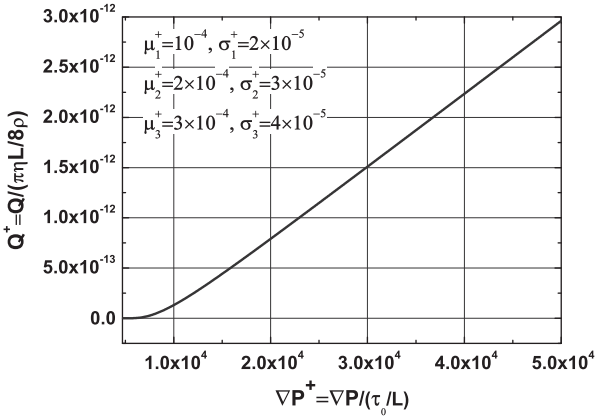

Fig. 8. Total flow rate vs. pressure gradient for a tri-modal distribution with $\mu_2^+ = 2\mu_1^+$, $\mu_3^+ = 3\mu_1^+$ and $\sigma_2^+ = 3\sigma_1^+/2$, $\sigma_3^+ = 2\sigma_1^+$ for a Bingham fluid.

$$q(\nabla P, r) = \begin{cases} \frac{\pi\tau_0 r^4}{4\eta r_0}\left[1 - \frac{16}{7}\left(\frac{r_0}{r}\right)^{1/2} + \frac{4}{3}\left(\frac{r_0}{r}\right) - \frac{1}{21}\left(\frac{r_0}{r}\right)^4\right] \text{ for } r > r_0 \\ 0 \quad \text{for } r \leqslant r_0 \text{ where } \tau_0 = \frac{\nabla P r_0}{2} \end{cases} \tag{15}$$

Similarly to the previous section, the total flow rate through a bundle of capillary tubes, the radii of which are distributed according to a probability density function $p(r)$, is obtained with the same

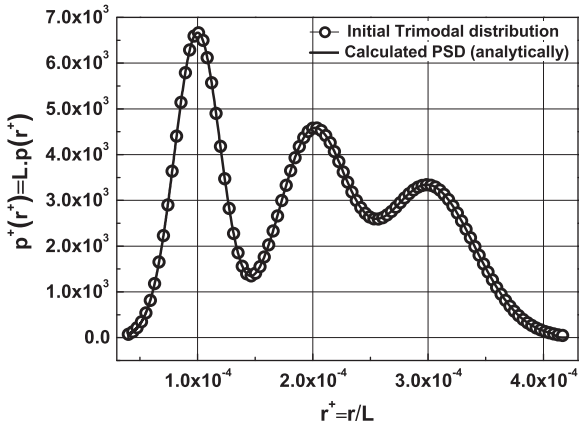

Fig. 9. Comparison between the initial and the calculated PSD for a tri-modal distribution with $\mu_2^+ = 2\mu_1^+$, $\mu_3^+ = 3\mu_1^+$ and $\sigma_2^+ = 3\sigma_1^+/2$, $\sigma_3^+ = 2\sigma_1^+$ for a Bingham fluid.

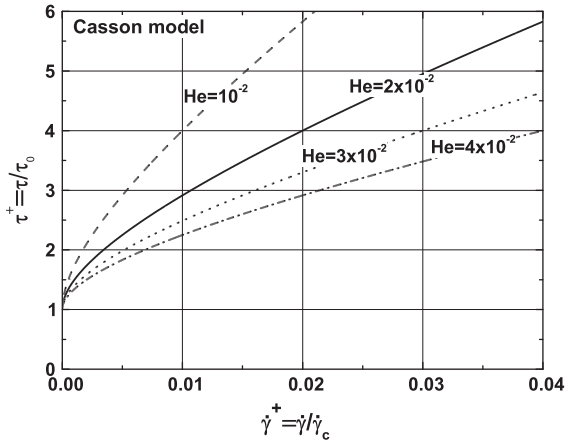

Fig. 10. Casson fluid rheograms for different *He*.

Volterra integral equation (Eq. (3)). The determination of $p(r)$ from this integral equation leads to the new dimensional PSDE:

$$p(r) = \frac{2\eta(\nabla P)^2}{\pi\tau_0 r^4}\left[\frac{15}{2}\frac{\partial^2.}{\partial(\nabla P)^2} + \frac{15}{2}\nabla P\frac{\partial^3.}{\partial(\nabla P)^3} + (\nabla P)^2\frac{\partial^4.}{\partial(\nabla P)^4}\right]Q|_{\nabla P=\frac{2\tau_0}{r}} \quad (16)$$

For the same reason justified above, we use the non-dimensional rheological behavior law of the Casson fluid:

$$\begin{cases} \left(\tau^+_{r'z}\right)^{1/2} = 1 + \frac{1}{He^{1/2}}\left|\frac{\partial u^+_z}{\partial r'^+}\right|^{1/2} \text{ for } \tau^+_{r'z} > 1 \\ \frac{\partial u^+_z}{\partial r'^+} = 0 \text{ for } \tau^+_{r'z} \leqslant 1 \end{cases} \quad (17)$$

where *He* is the same Hedström number as defined in the Bingham model. Then the non-dimensional kernel and PSD are given respectively by:

$$q^+(\nabla P^+, r^+) = \begin{cases} He\left[\nabla P^+(r^+)^4 - \frac{16\sqrt{2}}{7}(\nabla P^+)^{1/2}(r^+)^{7/2} + \frac{8}{3}(r^+)^3 - \frac{16}{21}\frac{1}{(\nabla P^+)^3}\right] & \text{for } r^+ > r_0^+ \\ 0 & \text{for } r^+ \leqslant r_0^+ \text{ where } r^+ = \frac{2}{\nabla P^+} \end{cases} \quad (18)$$

and

$$p^+(r^+) = \frac{(\nabla P^+)^6}{64He}\left[\frac{15}{2}\frac{\partial^2.}{\partial(\nabla P^+)^2} + \frac{15}{2}\nabla P^+\frac{\partial^3.}{\partial(\nabla P^+)^3} + (\nabla P^+)^2\frac{\partial^4.}{\partial(\nabla P^+)^4}\right]Q^+|_{\nabla P^+=\frac{2}{r^+}} \quad (19)$$

where all parameters are normalized as in Section 3.3. The adimensional rheograms are presented in Fig. 10 for different *He*. When the PSD is supposed to be the same Gaussian distribution as the one used in Section 3.3, the calculated total flow rate is shown in Fig. 11. In this figure we also compare the characteristic curves for the Bingham and Casson fluids. Notice that the normalized total flow rate for the Casson fluid exhibits a less steep evolution than for the Bingham fluid. Now, when Eq. (19) is applied to the Casson characteristic curve (Fig. 11), the initially injected Gaussian PSD is retrieved as we can see in Fig. 12.

Finally for the same tri-modal distribution as used above, the characteristic curve in Fig. 13 is obtained and once again the application of the new PSDE (Eq. (19)) gives the initial Gaussian tri-modal density probability function as shown in Fig. 14.

This method is therefore effective and robust and can be applied to all yield stress fluids (for example Herschel–Bulkley) and for all kinds of distributions.

4. Discussion

We propose a new technique in order to determine the pore size distribution based on the rheological properties of yield stress fluids such as Bingham, Casson or any other fluids of the same type. Like the previously quoted and described methods, this technique uses the capillary bundle model which, despite its apparent simplicity, is capable of characterizing the pore size distribution. Indeed the tortuosity of the percolating pores will introduce only a multiplying factor for the real flow rate but does not affect the type of the PSD [1,2]. For isotropic porous media, the flow rate in one particular direction is simply one third of the total flow rate and the PSD is not affected either as explained by Saffman [37]. In the case of pores whose radius varies along the flow path, the flow rate of yield stress fluids is controlled by the smallest pore section. Thus the measured distribution gives the PSD of the minimal pore size of each percolating conduit. As to the dead arms and the finite isolated clusters of pores, they do not take part in the flow and are not taken into account in the distribution. Finally the main weakness of this model is to neglect the interconnections between the percolating pores. We can nevertheless estimate that the measured PSD will be that of the pores presenting the minimum energy loss along the streamtube (corresponding to the shortest flow path and/or the largest radius). In conclusion, the model and the analysis adopted here are relevant as a first step in order to check the validity of our approach but aware of its weaknesses, we hope that this work can be extended to descriptions of more 3D realistic porous media using more sophisticated techniques such as homogenization [38]. The numerical and experimental validations of our model have been done by our team and co-workers [39]. Notice that because of the high order derivatives in Eqs. (11) and (19), we used a polynomial regression to filter the noise of the experimental data.

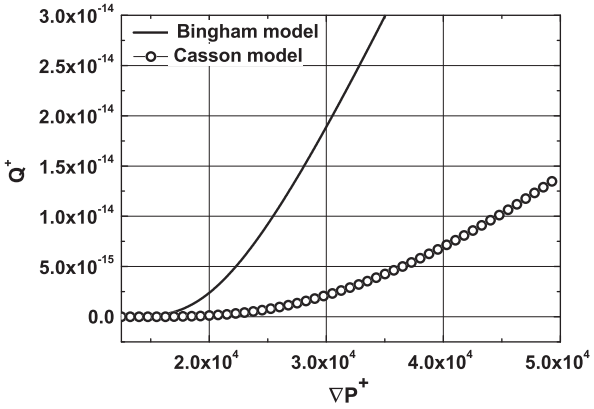

Fig. 11. Total flow rate vs. pressure gradient for a Gaussian distribution (Casson and Bingham fluids).

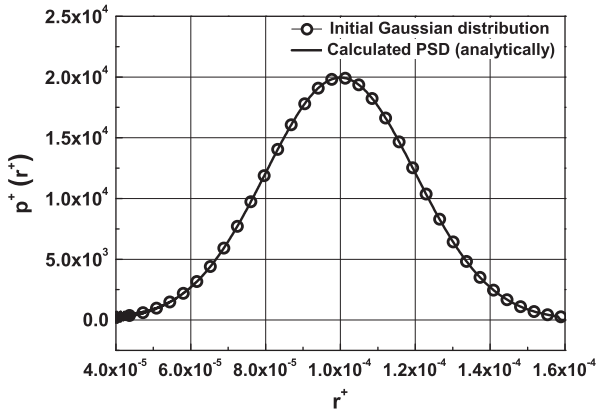

Fig. 12. Comparison between the initial and the calculated PSD for a Gaussian distribution and a Casson fluid.

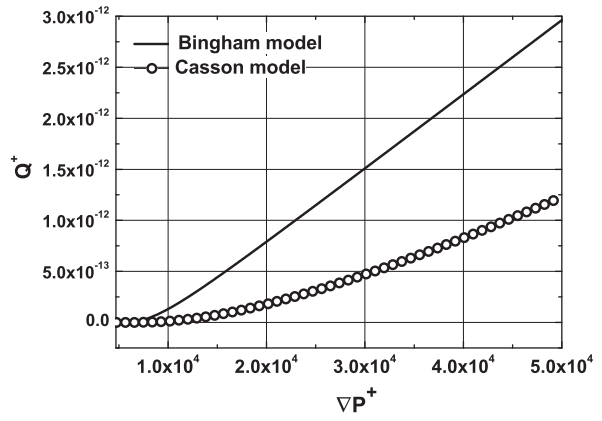

Fig. 13. Total flow rate vs. pressure gradient for a tri-modal distribution with $\mu_2^+ = 2\mu_1^+$, $\mu_3^+ = 3\mu_1^+$ and $\sigma_2^+ = 3\sigma_1^+/2$, $\sigma_3^+ = 2\sigma_1^+$ (Casson and Bingham fluids).

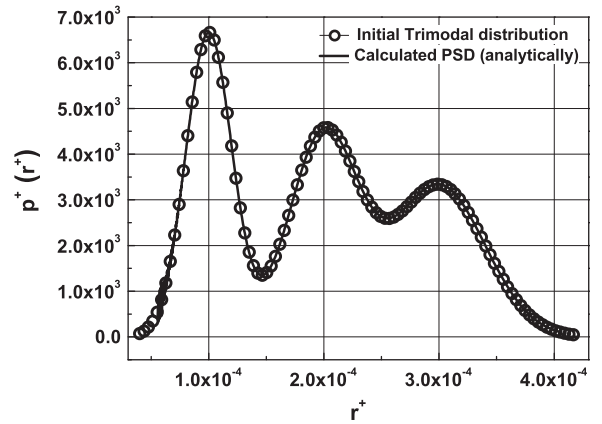

Fig. 14. Comparison between the initial and the calculated PSD for a tri-modal distribution with $\mu_2^+ = 2\mu_1^+$, $\mu_3^+ = 3\mu_1^+$ and $\sigma_2^+ = 3\sigma_1^+/2$, $\sigma_3^+ = 2\sigma_1^+$ for a Casson fluid.

This regression gives enough data to calculate accurately the high order derivatives.

5. Conclusion

This work presents a new method for determining the pore size distribution of porous media. It is based on the capillary bundle model like most of the alternative experimental techniques. The method rests on the existence of a yield stress in non-Newtonian pseudo-plastic fluids. This threshold gives the possibility of scanning the pore distribution and leads to a Volterra integral equation of the first kind whose kernel is analytically known. The mathematical determination of the probability density function $p(r)$ in this equation is done using the partial derivatives of the total flow rate of fluid through the porous medium as a function of the pressure gradient. This technique is successfully tested for Bingham and Casson fluids in the case of classical Gaussian and bi or tri-modal distributions. Nevertheless any other distribution or any other yield stress fluid could be used. It could become in the future an alternative, non-toxic and cheap method for the characterization of porous materials. An experimental validation of this approach is about to be published.

References

[1] F.A.L. Dullien, Porous Media – Fluid Transport and pore structure, second ed., Academic Press, 1992.
[2] A.E. Scheidegger, The Physics of Flow Through Porous Media, third ed., University of Toronto Press, 1974.
[3] M. Kaviany, Principles of Heat Transfer in Porous Media, second ed., Springer, 1995.
[4] P.M. Adler, Porous Media: Geometry and Transports, Butterworth-Heinemann, 1992.
[5] F.D. Winter, Solar Collectors, Energy Storage and Materials, MIT Press, Cambridge (Mass.), 1990.
[6] D. Zhou, C.Y. Zhao, Y. Tian, Review on thermal energy storage with phase change materials (PCMs) in building applications, Appl. Energy 92 (2012) 593–605.
[7] E.C. Donaldson, G.V. Chilingaria, T.F. Yen, Print Version: Enhanced Oil Recovery, II, Processes and Operations, Elsevier, Amsterdam; New York, 1989.
[8] K. Vafai, Porous Media: Applications in Biological Systems and Biotechnology, CRC Press: Taylor and Francis Group, 2011.
[9] H. Darcy, Les fontaines publiques de la ville de Dijon, Victor Dalmont, Paris, 1856.
[10] C.K. Ho, S.W. Webb, Theory and Application of Transport in Porous Media, Gas Transport, Springer 20 (2006).
[11] Z.E. Heinemann, Fluid flow in porous media, Textbook Ser. 1 (2003).
[12] E.P. Barrett, L.G. Joyner, P.P. Halenda, The determination of pore volume and area distributions in porous substances. Computations from nitrogen isotherms, J. Am. Chem. Soc. 73 (1951) 373–380.
[13] M. Wulff, Pore size determination by thermoporometry using acetonitrile, Thermochim. Acta 419 (2004) 291–294.
[14] T. Yamamoto, A. Ando, Y. Inagi, T. Ohmori, M. Nakaiwa, Evaluation of thermoporometry for characterization of mesoporous materials, J. Colloid Interface Sci. 284 (2005) 614–620.
[15] W. Kuhn, E. Peterli, H. Majer, Freezing point depression of gels produced by high polymer network, J. Polym. Sci. 16 (1955) 539–548.
[16] M. Brun, A. Lallemand, J-F Quinson, C. Eyraud, A new method for the simultaneous determination of the size and the shape of pores: the thermoporometry, Thermochim. Acta 21 (1977) 59–88.
[17] K. Ishikiriyama, M. Todoki, Pore size distribution measurements of silica gels by means of differential scanning calorimetry, J. Colloid Interface Sci. 171 (1995) 103–111.
[18] A.I. Sagidullin, I. Furo, Pore size distribution in small samples and with nanoliter volume resolution by NMR cryoporometry, Langmuir 24 (2008) 4470–4472.
[19] J.M. Haynes, Stereological analysis of pore structure, J. Mater. Struct. 6 (1973) 175–179.
[20] H. Ta mon, H. Is hizaka, SAXS study on gelation process in preparation of resorcinol-formaldehyde aerogel, J. Colloid Interface Sci. 206 (1998) 577–582.
[21] D. Pearson, A.J. Allen, A study of ultrafine porosity in hydrated cements using small angle neutron scattering, J. Mater. Sci. 20 (1985) 303–315.
[22] R.P. Chhabra, Bubbles, Drops, and Particles in Non-Newtonian Fluids, second ed., CRC Taylor and Francis, 2007.
[23] M. Benna, N. Kbir-Ariguib, A. Magnin, F. Bergaya, Effect of pH on rheological properties of purified Sodium Bentonite suspension, J. Colloid Interface Sci. 218 (1999) 442–455.
[24] E.C. Bingham, An investigation of the laws of plastic flow, US Bureau Stand. Bull. 13 (1916) 309–353.
[25] E.C. Bingham, Fluidity and Plasticity, McGraw-Hill Book Co., New York, 1922.
[26] E. Guyon, J.-P. Hulin, L. Petit, C.D. Mitescu, Physical Hydrodynamics, OUP Oxford, 2001.
[27] N. Casson, A flow equation for pigment-oil suspensions of the printing ink type, Br. Soc. Rheol. Proc. Rheol. Disperse Syst. (1959) 84–104.
[28] F. Yilmaz, M.Y. Gundogdu, A critical review on blood flow in large arteries; relevance to blood rheology viscosity models, and physiologic conditions, Korea–Australia Rheol. J. 20 (2008) 197–211.
[29] J. Kozeny, Uber kapillare Leitung des Wassers im Boden, Sitzungsberichte der Akademie der Wissenschaften in Wien 136 (2a) (1927) 106–271.

[30] P.C. Carman, Fluid flow through granular beds, Trans. Inst. Chem. Eng. 15 (1937) 154–155.
[31] E. Buckingham, On plastic flow through capillary tubes, Proc. Am. Soc. Test. Mater. (1921) 1154–1161.
[32] A. Ambari, M. Benhamou, S. Roux, E. Guyon, Pore size distribution in a porous medium obtained by a non-Newtonian fluid flow characteristic, C.R. Acad. Sci. Paris t. 311 (série II) (1990) 1291–1295.
[33] A. Oukhlef, A. Ambari, S. Champmartin, A. Despeyroux, Yield stress fluid method to measure the pore size distribution of a porous medium, in: Proceedings of ASME 2010, 3rd Joint US–European Fluids Engineering Summer Meeting and 8th International Conference on Nanochannels, Microchannels, and Minichannels, Montreal: Canada, 2010.
[34] R. Calvet, Le sol : propriétés et fonctions, Fr. Agric. Editions 1 (2003).
[35] B.O.A. Hedström, Flow of plastic materials in pipes, Ind. Eng. Chem. 44 (1952) 652–656.
[36] R.B. Bird, R.C. Armstrong, O. Hassager, Dynamics of Polymeric Liquids, second ed., John Wiley and Sons, New York, 1987.
[37] P.G. Saffman, A theory of dispersion in a porous medium, J. Fluid Mech. 6 (1959) 321–349.
[38] H. Hornung, Homogenization and Porous media, Springer, 1997.
[39] G. Malvault, A. Oukhlef, A.R.D. Castro, S. Champmartin, A. Ahmadi-Sénichault, A. Ambari, Nouvelle méthode de détermination de la distribution de la taille des pores d'un milieu poreux par l'injection d'un fluide à seuil, 11ème congrès de mécanique, Agadir: Maroc, 2013.